J. Fluid Mech. (1993), *vol.* 256, *pp.* 107–131

Near-contact thermocapillary motion of two non-conducting drops

By MICHAEL LOEWENBERG AND ROBERT H. DAVIS
Department of Chemical Engineering, University of Colorado, Boulder, CO 80309-0424, USA

(Received 16 November 1992 and in revised form 6 May 1993)

The axisymmetric, thermocapillary-driven motion of a pair of non-conducting, spherical drops in near contact is analysed for conditions of small Reynolds and Marangoni numbers. The pairwise motion and an associated contact force are computed by considering touching drops in point contact. Relative motion for nearly touching drops results from the contact force balanced by a lubrication resistance. A new, analytical solution is obtained for the axisymmetric temperature field around an unequal pair of non-conducting, tangent spheres embedded in an ambient temperature gradient. Numerical results for the pairwise migration velocity, contact force, and the relative and individual drop velocities are presented for all size ratios and a wide range of viscosity ratios, and asymptotic formulae are derived for small size ratios. For nearly equisized drops, the ratio of the relative velocity for two drops in near contact to that for widely separated drops is similar for thermocapillary-driven and gravity-driven motion. For small and moderate size ratios, however, this ratio is much larger for thermocapillary-driven relative motion than for gravity-driven relative motion, indicating that the former represents a more efficient coalescence mechanism. An explanation for this finding is provided in terms of the thermocapillary motion of the interface of the larger drop aiding the withdrawal of continuous phase from between the two drops.

1. Introduction

Predicting and controlling the microstructural properties of an emulsion of drops of one liquid phase finely dispersed in another liquid is an important goal in many chemical and materials processes. The drop size distribution in an emulsion evolves largely as the result of coalescence between droplets of the dispersed phase to form larger drops. On the microscale, coalescence results from pairwise relative motion between the drops. Under isothermal conditions in an unstirred, normal-gravity environment, buoyancy-driven migration is the primary source of the relative movement of drops larger than a few microns in diameter. In the presence of a temperature gradient, however, thermocapillary migration may dominate buoyancy migration, especially in reduced-gravity environments.

Although the focus of this paper is on thermocapillary motion, results for buoyancy motion are briefly reviewed first so that similarities and differences between the two cases may be demonstrated. Under low-Reynolds-number conditions, for which viscous forces dominate inertia, the buoyancy-driven migration velocity of an isolated spherical drop (denoted drop 1) through an unbounded solvent with viscosity μ is given by the Hadamard–Rybczynski formula (see Kim & Karilla 1991):

$$U_1^{G,0} = \frac{2a^2\Delta\rho}{3\mu}\frac{\lambda+1}{3\lambda+2}g, \tag{1.1}$$

where a and $\lambda\mu$ are the drop radius and viscosity, respectively, $\Delta\rho$ is the density difference between the drop and surrounding fluid, and g is the gravitational acceleration. The superscripts G and 0 refer to gravity motion and isolated drops, respectively. The buoyancy force acting on the drop is

$$F_1^G = \tfrac{4}{3}\pi a^3\Delta\rho g. \tag{1.2}$$

This force is balanced by the hydrodynamic, viscous drag on the drop, $F_1^{H,0} = -R_1^{H,0}U_1^{G,0}$, where the hydrodynamic resistance for an isolated drop is

$$R_1^{H,0} = 2\pi\mu a(3\lambda+2)/(\lambda+1). \tag{1.3}$$

Under the additional constraint of small Marangoni numbers, for which heat conduction dominates heat convection, the thermocapillary migration velocity of an isolated, non-conducting spherical drop is (Young, Goldstein & Block 1959)

$$U_1^{T,0} = \frac{a\beta}{\mu(3\lambda+2)}\nabla T_\infty, \tag{1.4}$$

where ∇T_∞ is the ambient temperature gradient and $\beta = -\partial\gamma/\partial T$ describes the temperature dependence of interfacial tension, γ, on the drop surface. The superscript T refers to thermocapillary motion. The interfacial tension for most (but not all) systems decreases with increasing temperature, indicating that drops migrate in the direction of increasing temperature. In contrast to buoyancy migration, there is no external force acting on a drop in thermocapillary migration; the drop 'swims' through the surrounding fluid as a result of the thrust generated by the interfacial tension gradient. Because of the linearity of the governing equations, however, we can consider the zero net external force to be the superposition of a 'thermocapillary force', $F_1^{T,0} = R_1^{T,0}\nabla T_\infty$, required to hold the drop stationary in a temperature gradient and the hydrodynamic force, $F_1^{H,0} = -R_1^{H,0}U_1^{T,0}$, on the drop translating at its thermocapillary migration velocity in an isothermal fluid. Using (1.3) and (1.4), the thermocapillary force on an isolated drop is

$$F_1^{T,0} = R_1^{T,0}\nabla T_\infty = \frac{2\pi a^2\beta}{\lambda+1}\nabla T_\infty. \tag{1.5}$$

A quantitative criterion for the relative importance of buoyancy-driven and thermocapillary-driven migration of isolated drops is given by the ratio of the velocities (1.1) and (1.4):

$$\frac{U_1^{T,0}}{U_1^{G,0}} = \frac{3}{2}\frac{\beta\nabla T_\infty}{a(\lambda+1)\Delta\rho g}. \tag{1.6}$$

This result indicates that thermocapillary-driven migration becomes increasingly important for smaller drops, drops of near-neutral buoyancy, strong temperature gradients, and reduced gravity environments.

The interactions of a pair of spherical drops in buoyancy-driven or thermocapillary-driven motion has been analysed by the method of reflections (Kim & Karrila 1991; Anderson 1985) and the method of images (Fuentes, Kim & Jeffrey 1988, 1989) for drops several radii apart. Solutions using bispherical coordinates (Rushton & Davies 1973; Haber, Hetsroni & Solan 1973; Zinchenko 1978, 1980; Keh & Chen 1990) and twin-spherical expansions (Satrape 1992) have been developed for smaller separations.

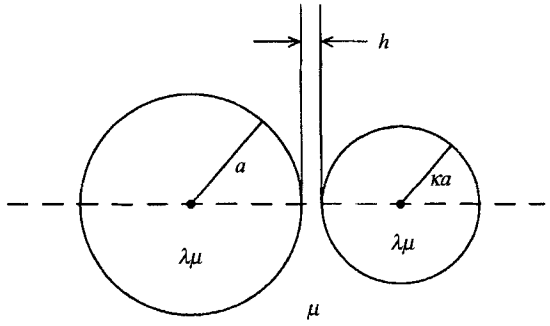

FIGURE 1. Defining sketch for two drops in close contact.

Unfortunately, bispherical-coordinate solutions and twin-spherical expansions become singular as the two drops come into contact; thus, the relative velocities between drops separated by a gap width, h, cannot be computed from these series solutions in the limit $h \to 0$.

Asymptotic analysis and lubrication theory have been used to describe the hydrodynamic resistance and relative motion of two drops moving parallel to their line of centres (Zinchenko 1983; Davis, Schonberg & Rallison 1989; Yiantsios & Davis 1991). The aim of the present work is to provide a similar description of the axisymmetric, near-contact motion of a droplet pair in thermocapillary-driven migration (figure 1) at small Reynolds and Marangoni numbers. The development is presented together with that for buoyancy-driven motion in order to elucidate the similarities and differences between the two mechanisms. The drops have radii $a_1 = a$ and $a_2 = \kappa a (0 < \kappa \leqslant 1)$. The distance h separating the drop surfaces is assumed small relative to either drop radius:

$$\epsilon \equiv h/\alpha \ll 1, \tag{1.7}$$

where $\alpha = \kappa a/(1+\kappa)$ is the reduced radius of the droplet pair. The continuous (suspending) and disperse phases are assumed to be Newtonian, incompressible fluids with viscosities μ and $\lambda\mu$, respectively. The suspending fluid is assumed to be unbounded and quiescent at infinity.

Appropriately defined, modified Bond numbers (Yiantsios & Davis 1991) are assumed to be sufficiently small that the drops remain spherical due to interfacial tension. The Péclet number for each drop is large compared to unity, so that Brownian motion is not considered. Non-hydrodynamic interdroplet forces such as van der Waals or electrostatic interactions are also not incorporated in the analysis. The drop surfaces are assumed to be clean and free of surfactant effects; thus, under isothermal conditions, the tangential component of the hydrodynamic stress is continuous across the drop surfaces. The various restrictions are generally met for drops with diameters between a few microns and a tenth of a millimetre, or so, depending on the physical parameters investigated (Zhang & Davis 1992). Under these conditions, the temperature field is decoupled from the velocity field and satisfies Laplace's equation:

$$\nabla^2 T(\boldsymbol{x}) = 0. \tag{1.8}$$

Far from the drops, a linear temperature distribution is assumed:

$$T(\boldsymbol{x}) - T_0 = \nabla T_\infty \cdot \boldsymbol{x} \quad (|\boldsymbol{x}| \to \infty), \tag{1.9}$$

where the applied temperature gradient, ∇T_∞, is parallel to the line of centres connecting the two drops, and T_0 is the temperature at the origin, which is located in

the small gap separating the drops. The thermal conductivity of the disperse phase is assumed to be much less than the conductivity of the suspending phase; hence, the drops may be treated as non-conducting:

$$\nabla T \cdot \boldsymbol{n} = 0 \quad \text{on the drop surfaces.} \tag{1.10}$$

The temperature field is continuous across the drop surfaces. The tangential stress balance on the drop surfaces is modified by this temperature field (Levich 1962, p. 384):

$$\hat{\sigma}_T - \sigma_T = -\nabla\gamma = \beta \nabla T \quad \text{on the drop surfaces,} \tag{1.11}$$

where σ_T and $\hat{\sigma}_T$ are the tangential components of hydrodynamic stress in the continuous and disperse phases. We note that ∇T is necessarily tangent to the surfaces of non-conducting drops because of (1.10).

In the following section (§2), we formulate expressions for drop velocities in terms of certain pairwise resistance functions and the lubrication resistance between two drops. Asymptotic formulae for the lubrication resistance are summarized in §3. A detailed scaling analysis is given in §4. An analytical solution for the axisymmetric temperature field external to an unequal pair of non-conducting, tangent spheres embedded in an ambient temperature gradient is given in §5. In §6, the numerical procedure for determining the velocity field away from the small gap separating two drops in an ambient temperature field is presented, and results for the pairwise migration velocity, contact force, and individual drop velocities are given in §7. Concluding remarks are provided in §8.

2. Problem formulation

We first review the theoretical development for the interaction of two drops in buoyancy-driven motion, and then present an analogous development for thermocapillary-driven motion. The force balance on each of two neighbouring drops translating along their line of centres under buoyancy-driven conditions is $F_i^G + F_i^H = 0$, where F_i^G and F_i^H are the components of the buoyancy and hydrodynamic forces, respectively, acting on each drop i parallel to the line of centres. The buoyancy force is $F_i^G = m_i g$, where $m_i = \frac{4}{3}\pi a_i^3 \Delta\rho$ is the mass of each drop i, minus the mass of fluid it displaces, and a_i is its radius. The hydrodynamic forces may be described in terms of resistance functions (Zinchenko 1978):

$$F_1^H = -A_{12}^H(U_1 - U_2) - A_{11}^H U_1, \quad F_2^H = -A_{22}^H(U_2 - U_1) - A_{21}^H U_1, \tag{2.1}$$

where U_1 and U_2 are the velocities of the two drops. The resistance functions satisfy a Lorentz-type reciprocal relation: $A_{12}^H = A_{22}^H - A_{21}^H$. The velocities are found by inverting these equations:

$$U_1^G = \left[\frac{m_1+m_2}{A_{11}^H + A_{21}^H} + \frac{A_{21}^H}{A_{11}^H + A_{21}^H}\,\frac{m_1 A_{21}^H - m_2 A_{11}^H}{A_{11}^H + A_{21}^H}\,\frac{1}{A_{22}^H - \dfrac{A_{21}^H A_{21}^H}{A_{11}^H + A_{21}^H}}\right] g, \tag{2.2a}$$

$$U_2^G = \left[\frac{m_1+m_2}{A_{11}^H + A_{21}^H} - \frac{A_{11}^H}{A_{11}^H + A_{21}^H}\,\frac{m_1 A_{21}^H - m_2 A_{11}^H}{A_{11}^H + A_{21}^H}\,\frac{1}{A_{22}^H - \dfrac{A_{21}^H A_{21}^H}{A_{11}^H + A_{21}^H}}\right] g. \tag{2.2b}$$

Although neutrally buoyant drops experiencing thermocapillary motion are force free, we may consider that this results from a balance of thermocapillary and hydrodynamic forces: $F_i^T + F_i^H = 0$. The hydrodynamic forces, F_i^H, are those acting on

each of two drops translating with velocities U_i^T through an unbounded, isothermal fluid. These hydrodynamic forces are given by (2.1). The thermocapillary forces, F_i^T, are those experienced by each of two stationary drops that are embedded in an ambient temperature gradient, ∇T_∞. Considering drops whose line of centres is aligned with the ambient temperature gradient, the thermocapillary forces have the form

$$F_i^T = \Lambda_i^T \nabla T_\infty, \tag{2.3}$$

where Λ_i^T is the thermocapillary resistance of drop i. Using (2.1), the thermocapillary migration velocity of each of a pair of force-free drops in an ambient temperature gradient is then

$$U_1^T = \left[\frac{\Lambda_1^T+\Lambda_2^T}{\Lambda_{11}^H+\Lambda_{21}^H}+\frac{\Lambda_{21}^H}{\Lambda_{11}^H+\Lambda_{21}^H}\frac{\Lambda_1^T\Lambda_{21}^H-\Lambda_2^T\Lambda_{11}^H}{\Lambda_{11}^H+\Lambda_{21}^H}\frac{1}{\Lambda_{22}^H-\dfrac{\Lambda_{21}^H\Lambda_{21}^H}{\Lambda_{11}^H+\Lambda_{21}^H}}\right]\nabla T_\infty, \tag{2.4a}$$

$$U_2^T = \left[\frac{\Lambda_1^T+\Lambda_2^T}{\Lambda_{11}^H+\Lambda_{21}^H}-\frac{\Lambda_{11}^H}{\Lambda_{11}^H+\Lambda_{21}^H}\frac{\Lambda_1^T\Lambda_{21}^H-\Lambda_2^T\Lambda_{11}^H}{\Lambda_{11}^H+\Lambda_{21}^H}\frac{1}{\Lambda_{22}^H-\dfrac{\Lambda_{21}^H\Lambda_{21}^H}{\Lambda_{11}^H+\Lambda_{21}^H}}\right]\nabla T_\infty. \tag{2.4b}$$

For the hypothetical case of two spherical drops in point contact ($\epsilon = 0$), $U_1 = U_2 = U_P$, where U_P is the pair migration velocity. In this case, the hydrodynamic resistance functions Λ_{11}^H and Λ_{21}^H are given by R_1^H and R_2^H, which describe the hydrodynamic resistances of each drop for pairwise translation in the point-contact configuration. Similarly, the thermocapillary resistances Λ_1^T and Λ_2^T are given by R_1^T and R_2^T, which describe the axisymmetric, thermocapillary resistances of two stationary, tangent drops embedded in an ambient temperature gradient. For tangent drops, the hydrodynamic and gravity or thermocapillary forces do not balance; a 'contact force', F_{12}, which acts on each drop with equal magnitude but opposite direction at their point of tangency completes the force balances:

$$m_1 g - R_1^H U_P^G - F_{12}^G = 0, \quad m_2 g - R_2^H U_P^G + F_{12}^G = 0, \tag{2.5}$$

$$R_1^T \nabla T_\infty - R_1^H U_P^T - F_{12}^T = 0, \quad R_2^T \nabla T_\infty - R_2^H U_P^T + F_{12}^T = 0. \tag{2.6}$$

These yield the pair migration velocities and contact forces for buoyancy and thermocapillary motion:

$$U_P^G = \frac{m_1+m_2}{R_1^H+R_2^H}g, \quad U_P^T = \frac{R_1^T+R_2^T}{R_1^H+R_2^H}\nabla T_\infty, \tag{2.7}$$

$$F_{12}^G = \frac{m_1 R_2^H - m_2 R_1^H}{R_1^H+R_2^H}g, \quad F_{12}^T = \frac{R_1^T R_2^H - R_2^T R_1^H}{R_1^H+R_2^H}\nabla T_\infty. \tag{2.8}$$

Away from the gap separating drops in near contact ($\epsilon \ll 1$), the temperature and velocity fields can be computed to $O(\epsilon)$ by considering tangent drops as described above. In the gap, each field is sensitive to the gap width, but its contribution to the overall hydrodynamic and thermocapillary resistances is very slight. Thus,

$$\Lambda_{11}^H = R_1^H + O(\epsilon), \quad \Lambda_{21}^H = R_2^H + O(\epsilon) \quad (\epsilon \ll 1), \tag{2.9}$$

$$\Lambda_1^T = R_1^T + O(\epsilon), \quad \Lambda_2^T = R_2^T + O(\epsilon) \quad (\epsilon \ll 1), \tag{2.10}$$

as demonstrated in §6.2. For drops in near contact, the limiting form of the individual drop velocities given by (2.4) can be expressed in terms of the pair migration velocity and the deviation velocities due to a resistance equal (within $O(\epsilon)$) to the contact force:

$$U_1 = U_P + \frac{R_2^H}{R_1^H+R_2^H}\frac{F_{12}}{R_{12}^H}, \quad U_2 = U_P - \frac{R_1^H}{R_1^H+R_2^H}\frac{F_{12}}{R_{12}^H}, \tag{2.11}$$

where R_{12}^H is the lubrication resistance defined by

$$R_{12}^H = \lim_{\epsilon \to 0} \left[A_{22}^H - \frac{A_{21}^H A_{21}^H}{A_{11}^H + A_{21}^H} \right]. \tag{2.12}$$

The relative motion of the two drops along their line of centres is simply

$$U_{12} \equiv U_1 - U_2 = F_{12}/R_{12}^H. \tag{2.13}$$

3. Lubrication resistance between two drops

The spherical drops, asymptotic formulae for the lubrication resistance in the limit $\epsilon \to 0$ are given by (Davis *et al.* 1989; Zinchenko 1983):

$$R_{12}^H = \frac{6\pi\mu\alpha}{\epsilon} \frac{\lambda^2\epsilon + 0.402\lambda\epsilon^{\frac{1}{2}}}{\lambda^2\epsilon + 1.711\lambda\epsilon^{\frac{1}{2}} + 0.461} \qquad (\lambda\epsilon^{\frac{1}{2}} \gg \epsilon \ln \epsilon^{-1}), \tag{3.1}$$

$$R_{12}^H = 6\pi\mu\alpha \left[\frac{\pi^2}{16} \lambda \left(\frac{2}{\epsilon} \right)^{\frac{1}{2}} + \frac{3-\lambda^2}{9} \ln \epsilon^{-1} + C(\kappa, \lambda) \right] \quad (\lambda\epsilon^{\frac{1}{2}} \ll 1), \tag{3.2}$$

where $C(\kappa, \lambda)$ is an $O(1)$ constant given by Zinchenko (1982). For bubbles ($\lambda = 0$), some representative values are $C = \frac{1}{3}(2\gamma_E + \ln 2) = 0.616$ (minimum value) for $\kappa = 0$, $C = \frac{2}{3}(\gamma_E + \ln 2) = 0.847$ for $\kappa = 1$, and $C = 0.878$ (maximum value) for $\kappa = 0.678$, where $\gamma_E = 0.577\ldots$ is Euler's constant; values for $\lambda = O(1)$ are similar and are tabulated by Zhang & Davis (1991).

Three distinguishing limits can be identified from the above formulae:

$$R_{12}^H = 6\pi\mu\alpha\epsilon^{-1} \qquad (\lambda\epsilon^{\frac{1}{2}} \gg 1), \tag{3.3}$$

$$R_{12}^H = \tfrac{8}{3}\pi^3 \mu\lambda\alpha(2/\epsilon)^{\frac{1}{2}} \qquad (1 \gg \lambda\epsilon^{\frac{1}{2}} \gg \epsilon \ln \epsilon^{-1}), \tag{3.4}$$

$$R_{12}^H = 2\pi\mu\alpha[\ln \epsilon^{-1} + 3C(\kappa, 0)] \quad (\lambda\epsilon^{\frac{1}{2}} \ll \epsilon \ln \epsilon^{-1}), \tag{3.5}$$

which correspond, respectively, to immobile drop interfaces (i.e. rigid particles, or drops with surfactant), 'fully-mobile' interfaces, and to free (i.e. bubble) interfaces. Note that the drop viscosity does not affect the lubrication resistance for immobile or free interfaces, whereas the continuous-phase viscosity is unimportant for fully mobile interfaces. A uniformly valid estimate of the lubrication resistance for arbitrary viscosity ratio is given by

$$\frac{\epsilon R_{12}^H}{\mu\alpha} = O\left(\frac{\lambda\epsilon^{\frac{1}{2}} + \epsilon \ln \epsilon^{-1}}{\lambda\epsilon^{\frac{1}{2}} + 1} \right), \tag{3.6}$$

which incorporates the above limits and aids the following scaling analysis.

4. Scaling analysis

4.1. *Nearly equisized drops:* $1-\kappa \ll 1$

For $1-\kappa \ll 1$, the resistances of two nearly equal drops differ from each other by only $O(1-\kappa)$. Noting also that $m_1/m_2 = 1 + 3(1-\kappa) + O(1-\kappa)^2$, (2.7), (2.8), and (2.11) yield the following qualitative results for both buoyancy and thermocapillary motion of two drops in near contact ($\epsilon \ll 1$)

$$\epsilon^{-1} \frac{\lambda\epsilon^{\frac{1}{2}} + \epsilon \ln \epsilon}{\lambda\epsilon^{\frac{1}{2}} + 1} \frac{U_{12}}{U_1^0} = O\left(\frac{F_{12}}{F_1^0} \right) = O(1-\kappa) \quad (1-\kappa \ll 1), \tag{4.1}$$

$$\frac{U_P}{U_{EQ}} = O\left(\frac{U_1 - U_P}{U_P - U_2} \right) = 1 + O(1-\kappa) \quad (1-\kappa \ll 1), \tag{4.2}$$

where U_{EQ} is the migration velocity of an equisized pair and R_{12}^H was estimated using (3.6). Recall also that the superscript 0 denotes an isolated drop. As expected, the relative velocity and mutual contact force vanish for $1-\kappa \to 0$, and the deviation velocities are nearly equal. The mutual hydrodynamic shielding of an equisized droplet pair implies that $R_1^H < R_1^{H,0}$. The minimum theorem of Hill & Power (1956) states that the hydrodynamic resistance of a body exceeds that of all bodies that can be completely enclosed within its surface; thus, $\frac{1}{2}R_1^{H,0} < R_1^H$. Similarly, it follows that $\frac{1}{2}R_1^{T,0} < R_1^T < R_1^{T,0}$ for equisized drops. Thus, according to (2.7),

$$1 < U_{EQ}^G/U_1^{G,0} < 2, \quad \tfrac{1}{2} < U_{EQ}^T/U_1^{T,0} < 2 \quad (1-\kappa \ll 1). \tag{4.3}$$

4.2. *Small size ratios:* $\kappa \ll 1$

For $\kappa \ll 1$, the flow field past a tangent pair of drops is dominated by the flow field associated with the isolated migration of the larger drop. An areal fraction, κ^2, of the larger drop surface at the stagnation point is shielded by the presence of the smaller drop. Since stresses are approximately uniform on the drop surface, the shielding by the smaller drop reduces the hydrodynamic and thermocapillary resistance on the larger drop in proportion to the fraction shielded. Thus, the pair migration velocity is

$$U_P/U_1^0 = 1+O(\kappa^2), \tag{4.4}$$

for both buoyancy-driven and thermocapillary-driven motion.

The hydrodynamic force on the smaller drop is estimated as

$$F_2^H = O[\mu\kappa a u_r(\boldsymbol{x}_2)], \tag{4.5}$$

where $u_r(\boldsymbol{x}_2)$ is the radial component of the velocity field associated with the isolated migration of the larger drop evaluated at the centre of the smaller drop. Expanding the Hadamard–Rybczynski velocity field in spherical coordinates about the surface of the large drop at $r = a$, we obtain

$$u_r^G = -\frac{U_1^{G,0}}{\lambda+1}[\delta+(\tfrac{3}{2}\lambda-1)\,\delta^2+O(\delta^3)]\cos\theta, \tag{4.6a}$$

$$u_\theta^G = -\frac{1}{2}\frac{U_1^{G,0}}{\lambda+1}[1+(3\lambda+1)\,\delta+O(\delta^2)]\sin\theta, \tag{4.6b}$$

where $\delta = (r-a)/a \ll 1$. Evaluating this expression at the centre of the smaller drop ($\delta = \kappa, \theta = 0$) and inserting the result into (4.5) yields an estimate for the hydrodynamic resistance on the smaller drop. Estimates for the two drops which are uniformly valid in λ are thus

$$\frac{R_1^H}{R_1^{H,0}} = 1-O(\kappa^2), \quad \frac{R_2^H}{R_1^{H,0}} = O\left(\kappa^2\frac{\kappa\lambda+1}{\lambda+1}\right) \qquad (\kappa \ll 1). \tag{4.7}$$

Inserting the estimates (4.4) and (4.7) into the force balance (2.5) for the smaller drop yields an estimate of the mutual contact force for buoyancy-driven motion of a pair with disparate sizes:

$$\frac{F_{12}^G}{F_1^G} = O\left(\kappa^2\frac{\kappa\lambda+1}{\lambda+1}\right) \quad (\kappa \ll 1). \tag{4.8}$$

Note that $F_{12}^G \approx F_2^H \gg F_2^G$ for small and moderate viscosity ratios ($\kappa\lambda \ll 1$), whereas $F_{12}^G = O(F_2^H) = O(F_2^G)$ for rigid spheres and highly viscous drops ($\kappa\lambda \gg 1$).

For $\kappa \ll 1$, the thermocapillary-driven contact force is estimated from the force experienced by a smaller drop that is tangent to the stagnation point of a larger drop undergoing thermocapillary-driven migration. We will show that the force experienced by the smaller drop due to the velocity field produced by the larger drop dominates that due to interfacial tension gradients on the smaller drop. Thermocapillary motion is force free and torque free; thus, the net velocity field generated by the migration of an isolated drop is a potential flow field. Expanding the potential field about the surface of the larger drop at $r = a$ yields

$$u_r^T = -3U_1^{T,0}[\delta + O(\delta^2)]\cos\theta, \tag{4.9a}$$

$$u_\theta^T = -\tfrac{3}{2}U_1^{T,0}[1 + O(\delta)]\sin\theta, \tag{4.9b}$$

where $\delta = (r-a)/a \ll 1$. Evaluating this solution at the centre of the smaller drop ($\delta = \kappa, \theta = 0$) and employing (4.5) yields

$$\frac{F_2^T}{F_1^{T,0}} = O(\kappa^2) = \frac{F_{12}^T}{F_1^{T,0}} = O\left(\frac{\lambda+1}{\kappa\lambda+1}\frac{F_{12}^G}{F_1^G}\right) \quad (\kappa \ll 1), \tag{4.10}$$

where $F_1^{T,0}$ is the thermocapillary force given by (1.5) for the larger drop when isolated. Using (1.5) and the temperature field around an isolated, non-conducting drop, it is seen that the force due to interfacial tension gradients on the smaller drop is $O(\kappa^3 F_1^{T,0})$ for $\kappa \ll 1$, which is dominated by the force due to the velocity field of the large drop. Thus, $F_{12}^T = F_2^T[1 + O(\kappa)]$, as claimed above.

If $\kappa \ll 1$ and $\lambda \gg 1$, then (2.5), (4.7), and (4.8) indicate that $U_P^G > U_1^{G,0}$ (i.e. the larger drop speeds up due to the presence of the smaller drop) since the $O(\kappa^2)$ reduction of R_1^H dominates F_{12}^G. However, the sign of $U_P^G - U_1^{G,0}$ is uncertain if $\lambda \leqslant O(1)$, since the reduction of R_1^H is then comparable to F_{12}^G. Similarly, the sign of $U_P^T - U_1^{T,0}$ cannot be predicted, since the reduction of R_1^H and R_1^T are both $O(F_{12}^T)$. In all cases, the consistency of (4.4) is apparent.

Combining (4.8) and (4.10) with (1.3), (2.13) and (3.6) yields the relative drop velocities for $\kappa \ll 1$:

$$\frac{U_{12}^T}{U_1^{T,0}} = O\left(\frac{\lambda+1}{\kappa\lambda+1}\frac{U_{12}^G}{U_1^{G,0}}\right) = O\left(\epsilon\kappa\frac{\lambda\epsilon^{\frac{1}{2}}+1}{\lambda\epsilon^{\frac{1}{2}}+\epsilon\ln\epsilon^{-1}}\right) \quad (\kappa \ll 1). \tag{4.11}$$

When $\lambda \gg 1$, the relative gravitational velocity is reduced from the pairwise velocity by a much greater factor than is the relative thermocapillary velocity. Finally, the estimates of (4.7) are inserted into (2.11) to yield

$$\frac{U_1^T - U_P^T}{U_P^T - U_2^T} = \frac{U_1^G - U_P^G}{U_P^G - U_2^G} = O\left(\kappa^2\frac{\kappa\lambda+1}{\lambda+1}\right) \quad (\kappa \ll 1), \tag{4.12}$$

indicating that the relative velocity of the drops is due almost entirely to the deviation of the smaller drop velocity relative to the pairwise motion.

An important *quantitative* relationship between buoyancy-driven and thermocapillary-driven motion may be derived for the case $\kappa(\lambda+1) \ll 1$. A comparison of (4.6) and (4.9) reveals that

$$\boldsymbol{u}^G/U_1^{T,0} = 3(\lambda+1)\boldsymbol{u}^T/U_1^{G,0} + O(\kappa(\lambda+1)) \quad (\kappa(\lambda+1) \ll 1). \tag{4.13}$$

It therefore follows that the hydrodynamic forces, F_2^H and F_2^T, acting on the smaller

drop in buoyancy-driven and thermocapillary-driven motion, respectively, obey the quantitative relationship

$$F_2^T/F_1^{T,0} = 3(\lambda+1)F_2^H/F_1^G \quad (\kappa(\lambda+1) \ll 1). \tag{4.14}$$

Then, according to (4.8), the remark following (4.10), and (2.13), we have

$$F_{12}^T/F_{12}^G = U_{12}^T/U_{12}^G = 3(\lambda+1)\,U_1^{T,0}/U_1^{G,0} \quad (\kappa \ll 1, \quad \kappa\lambda \ll 1). \tag{4.15}$$

For $\lambda\kappa \gg 1$, (4.8), (4.10), and (2.13) yields

$$F_{12}^T/F_{12}^G = U_{12}^T/U_{12}^G = O(\kappa^{-1}U_1^{T,0}/U_1^{G,0}) \quad (\kappa \ll 1, \quad \kappa\lambda \gg 1). \tag{4.16}$$

In contrast to the result, (4.1), for $1-\kappa \ll 1$, (4.15) and (4.16) predict that the ratio of the thermocapillary and gravitational relative velocities of two nearly touching drops for $\lambda \gg 1$, $\kappa \ll 1$ is significantly greater than the ratio of isolated drop velocities given by (1.6). This prediction is quantified by numerical calculations; the results are given by (7.8)–(7.10).

5. Temperature field surrounding two non-conducting spheres

5.1. *Tangent-sphere formulation*

The problem of two non-conducting, tangent spheres in an ambient temperature gradient is formulated in tangent-sphere coordinates (η, ν, ϕ), as depicted in figure 2 and described by Moon & Spencer (1961, p. 104). This coordinate system is a right-handed, orthogonal, curvilinear coordinate system related to a cylindrical coordinate system (z, ρ, θ) by

$$z = \frac{\eta}{\eta^2+\nu^2}, \quad \rho = \frac{\nu}{\eta^2+\nu^2}, \quad \theta = \phi. \tag{5.1}$$

Thus, the origin is at the point of contact between the tangent spheres, and the distance from the origin is given by $r = (\rho^2+z^2)^{\frac{1}{2}} = 1/(\eta^2+\nu^2)^{\frac{1}{2}}$. In this coordinate system, tangent spheres of radii a and κa with centres on the z-axis at $z = -a$ and $z = +\kappa a$ are defined by the constant coordinate surfaces

$$\eta = -\eta_1 = -\frac{1}{2a} \quad \text{(sphere 1)}, \qquad \eta = \eta_2 = \frac{1}{2\kappa a} \quad \text{(sphere 2)}, \tag{5.2}$$

and the conjugate coordinate surfaces, ν = constant, are tori with zero inner radii.

For non-conducting drops, the temperature field is conveniently solved using a stream function, ψ, to define the temperature gradient by analogy to the customary definition of an incompressible, axisymmetric velocity field (Sadhal 1983; Feuillebois 1989; D. J. Jeffrey, personal communication). Accordingly, the components of the temperature gradient are given by (Kim & Karrila 1991, p. 97)

$$(\nabla T)_\eta = -\frac{1}{\nu}(\eta^2+\nu^2)^2\frac{\partial\psi}{\partial\nu}, \quad (\nabla T)_\nu = \frac{1}{\nu}(\eta^2+\nu^2)^2\frac{\partial\psi}{\partial\eta}. \tag{5.3}$$

Since the temperature field and a potential-flow velocity field both satisfy Laplace's equation (1.8) and boundary conditions (1.9) and (1.10), the two fields are mathematically identical. Accordingly, the stream function that defines the temperature field satisfies

$$\mathrm{E}^2\psi = (\eta^2+\nu^2)\left(\nu\frac{\partial}{\partial\nu}\left\{\frac{1}{\nu}\frac{\partial}{\partial\nu}[\psi(\eta^2+\nu^2)^{\frac{1}{2}}]\right\}+\frac{\partial^2}{\partial\eta^2}[\psi(\eta^2+\nu^2)^{\frac{1}{2}}]\right) = 0, \tag{5.4}$$

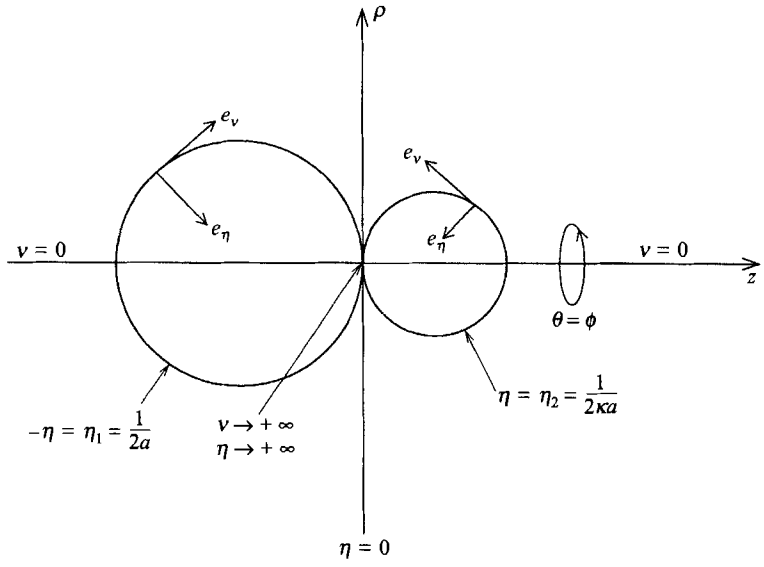

FIGURE 2. Tangent-sphere coordinates for two spheres in point contact.

with boundary conditions

$$\psi = \frac{1}{2}\left(\frac{\nu}{\eta^2+\nu^2}\right)^2 \nabla T_\infty, \quad \eta^2+\nu^2 \to 0, \tag{5.5}$$

$$\psi = 0, \quad \eta = -\eta_1, +\eta_2, \tag{5.6}$$

where η_1 and η_2 are given by (5.2). Equations (5.4)–(5.6) are separable in tangent sphere coordinates. If we substitute a solution of the form

$$\psi = \frac{M(\eta)\,N(\nu)}{(\eta^2+\nu^2)^{\frac{1}{2}}} \tag{5.7}$$

into (5.4), we obtain ordinary differential equations for M and N:

$$\frac{\mathrm{d}^2M}{\mathrm{d}\eta^2} - s^2M = 0, \quad \nu^2\frac{\mathrm{d}^2N}{\mathrm{d}\nu^2} - \nu\frac{\mathrm{d}N}{\mathrm{d}\nu} + s^2\nu^2N = 0, \tag{5.8}$$

where s is a continuously valued separation constant: $0 \leqslant s < \infty$. The solutions are

$$M = c_1 \sinh s\eta + c_2 \cosh s\eta, \quad N = c_3\,\nu J_1(s\nu) + c_4\,\nu Y_1(s\nu), \tag{5.9}$$

where J_1 and Y_1 are first-order Bessel functions of the first and second kind, respectively. Since $Y_1(s\nu)$ is singular at $\nu = 0$, the entire z-axis external to the spheres, this solution is eliminated: $c_4 = 0$.

A general, non-singular solution of (5.4) that satisfies (5.5) is

$$\psi = \frac{\nu}{(\eta^2+\nu^2)^{\frac{1}{2}}}\int_0^\infty [X(s)\sinh s\eta + Z(s)\cosh s\eta]\,J_1(s\nu)\,\mathrm{d}s + \frac{1}{2}\left(\frac{\nu}{\eta^2+\nu^2}\right)^2 \nabla T_\infty, \tag{5.10}$$

where $X(s)$ and $Z(s)$ are functions that are determined from the boundary conditions

on the drop surfaces. The procedure for determining $X(s)$ and $Z(s)$ is facilitated by the identity (Erdelyi *et al.* 1954):

$$\frac{\nu}{(\eta^2+\nu^2)^{\frac{3}{2}}} = \int_0^\infty s\,\mathrm{e}^{-s|\eta|} J_1(s\nu)\,\mathrm{d}s, \tag{5.11}$$

which allows (5.10) to be rewritten as

$$\psi = \frac{\nu}{(\eta^2+\nu^2)^{\frac{1}{2}}} \int_0^\infty [X(s)\sinh s\eta + Z(s)\cosh s\eta + \tfrac{1}{2}s\,\mathrm{e}^{-s|\eta|}\nabla T_\infty] J_1(s\nu)\,\mathrm{d}s. \tag{5.12}$$

The remaining boundary conditions, (5.6), are thus reduced to

$$-X(s)\sinh s\eta_1 + Z(s)\cosh s\eta_1 = -\tfrac{1}{2}s\,\mathrm{e}^{-s\eta_1}\nabla T_\infty, \tag{5.13}$$

$$X(s)\sinh s\eta_2 + Z(s)\cosh s\eta_2 = -\tfrac{1}{2}s\,\mathrm{e}^{-s\eta_2}\nabla T_\infty. \tag{5.14}$$

These are inverted to yield

$$X(s) = -\frac{s}{2}\frac{\sinh s(\eta_1-\eta_2)}{\sinh s(\eta_1+\eta_2)}\nabla T_\infty, \quad Z(s) = s\left[\frac{\sinh s\eta_1 \sinh s\eta_2}{\sinh s(\eta_1+\eta_2)} - \frac{1}{2}\right]\nabla T_\infty. \tag{5.15}$$

Substituting (5.15) into (5.10) yields an analytical solution for the axisymmetric temperature field external to non-conducting, tangent spheres ($0 \leqslant \eta_1, \eta_2 < \infty$). Far from the droplet pair ($\eta^2+\nu^2 \to 0$), the integral term in (5.10) describes a dipole disturbance. The temperature gradient on the drop surfaces is obtained according to (5.3) while making explicit use of (5.6); the result is

$$\frac{(\nabla T)_{\nu,1}}{\nabla T_\infty} = (\eta_1^2+\nu^2)^{\frac{3}{2}} \int_0^\infty \frac{\sinh s\eta_2}{\sinh s(\eta_1+\eta_2)} s^2 J_1(s\nu)\,\mathrm{d}s \quad \text{(drop 1)}, \tag{5.16}$$

$$\frac{(\nabla T)_{\nu,2}}{\nabla T_\infty} = -(\eta_2^2+\nu^2)^{\frac{3}{2}} \int_0^\infty \frac{\sinh s\eta_1}{\sinh s(\eta_1+\eta_2)} s^2 J_1(s\nu)\,\mathrm{d}s \quad \text{(drop 2)}, \tag{5.17}$$

and $(\nabla T)_\eta = 0$ for $\eta = -\eta_1$ and $\eta = \eta_2$, as required for non-conducting drops.

5.2. *Temperature field near the contact point*

We now determine the asymptotic behaviour of the temperature gradient on the surface of non-conducting, tangent drops near the contact point. The results of this analysis are needed in §6 for determining the flow field in the near-contact region.

Rewriting (5.16) using $J_0'(x) = -J_1(x)$ and an integral representation (Abramowitz & Stegun 1972, pp. 358–378) for $J_0(x)$, we obtain the following expression for the temperature gradient on the surface of drop 1:

$$\frac{(\nabla T)_{\nu,1}}{\nabla T_\infty} = (\eta_1^2+\nu^2)^{\frac{3}{2}} \frac{\mathrm{d}}{\mathrm{d}\nu} \int_0^\infty \frac{s\sinh s\eta_2}{\sinh s(\eta_1+\eta_2)} \left(\frac{2}{\pi}\int_1^\infty \frac{\mathrm{i}\,\mathrm{e}^{\mathrm{i}s\nu t}}{(t^2-1)^{\frac{1}{2}}}\,\mathrm{d}t\right)\mathrm{d}s, \tag{5.18}$$

where the temperature gradient is given by the real part of the integrand. Since this is an even function of s, we can rearrange (5.18):

$$\frac{(\nabla T)_{\nu,1}}{\nabla T_\infty} = \frac{\mathrm{i}}{\pi}(\eta_1^2+\nu^2)^{\frac{3}{2}} \frac{\mathrm{d}}{\mathrm{d}\nu} \int_1^\infty \frac{\mathrm{d}t}{(t^2-1)^{\frac{1}{2}}} \int_{-\infty}^\infty \frac{s\sinh s\eta_2\,\mathrm{e}^{\mathrm{i}s\nu t}}{\sinh s(\eta_1+\eta_2)}\,\mathrm{d}s. \tag{5.19}$$

By Jordan's Lemma (Carrier, Krook & Pearson 1966, pp. 77–101), the integral over s can be determined from an integral in the complex plane on a contour that includes

the real axis and a semicircle in the upper half-plane. The integrand has a removable singularity at $s = 0$ (simple pole with zero residue) and simple poles at

$$s_k = \frac{\mathrm{i}k\pi}{\eta_1+\eta_2} \quad (k = 1, 2, 3, \ldots, \infty), \tag{5.20}$$

with residues

$$\mathrm{res}_k = -\frac{k\pi(-1)^k}{(\eta_1+\eta_2)^2}\sin\left(\frac{k\pi\eta_2}{\eta_1+\eta_2}\right)\exp\left[-\frac{k\pi\nu t}{\eta_1+\eta_2}\right]. \tag{5.21}$$

Using the residue theorem (Carrier *et al.* 1966, pp. 77–101), we find

$$\frac{(\nabla T)_{\nu,1}}{\nabla T_\infty} = 2\pi\frac{(\eta_1^2+\nu^2)^{\frac{3}{2}}}{(\eta_1+\eta_2)^2}\sum_{k=1}^{\infty} k(-1)^k \sin\left(\frac{k\pi\eta_2}{\eta_1+\eta_2}\right)\frac{\mathrm{d}}{\mathrm{d}\nu}\int_1^\infty \frac{\exp\left[-\dfrac{k\pi\nu t}{\eta_1+\eta_2}\right]}{(t^2-1)^{\frac{1}{2}}}\mathrm{d}t. \tag{5.22}$$

Then, recognizing the integral representation for the modified Bessel function, $K_0(x)$, and using the relationship $K_0'(x) = -K_1(x)$, allows the surface temperature gradient to be expressed as

$$\frac{(\nabla T)_{\nu,1}}{\nabla T_\infty} = -2\pi^2\left(\kappa\frac{(1+4a^2\nu^2)^{\frac{1}{2}}}{1+\kappa}\right)^3\sum_{k=1}^{\infty} k^2(-1)^k\sin\left(\frac{k\pi}{1+\kappa}\right)K_1\left(\frac{2k\pi\kappa a\nu}{1+\kappa}\right), \tag{5.23}$$

where we have used (5.2). A similar expression is obtained for the temperature gradient on the smaller sphere surface:

$$\frac{(\nabla T)_{\nu,2}}{\nabla T_\infty} = 2\pi^2\left(\frac{(1+4\kappa^2a^2\nu^2)^{\frac{1}{2}}}{1+\kappa}\right)^3\sum_{k=1}^{\infty} k^2(-1)^k\sin\left(\frac{k\pi\kappa}{1+\kappa}\right)K_1\left(\frac{2k\pi\kappa a\nu}{1+\kappa}\right). \tag{5.24}$$

The tangential extent of the near-contact region between the drops is given by $\rho = O(\alpha\epsilon^{\frac{1}{2}})$ (Davis *et al.* 1989). Thus, according to (5.1) and figure 2, the near-contact region of the drop surfaces is defined by

$$\alpha\nu = O(\epsilon^{-\frac{1}{2}})\,(\epsilon \ll 1), \quad \eta = -\eta_1, \eta_2. \tag{5.25}$$

To examine the gradient on the drop surfaces near the contact point, we consider (5.23) and (5.24) in the limit described by (5.25). The result is

$$\frac{(\nabla T)_{\nu,1}}{\nabla T_\infty} = -\frac{(\nabla T)_{\nu,2}}{\nabla T_\infty} = 16\pi x^{\frac{5}{2}}\sin\left(\frac{\pi}{1+\kappa}\right)\mathrm{e}^{-2\pi x} \quad (x = \alpha\nu \geqslant O(\epsilon^{-\frac{1}{2}})), \tag{5.26}$$

where we have used the identity $\lim_{t\to\infty} K_1(t) = (2/\pi t)^{\frac{1}{2}}\mathrm{e}^{-t}$. Hence, we conclude that $(\nabla T)_\nu$ is exponentially small on the near-contact portion of the drop surfaces.

6. Solution of the flow field for pairwise motion

6.1. *Tangent-sphere formulation*

The solution for the flow fields inside and outside two touching drops is formulated using the tangent-sphere coordinates described in the previous section. Under the low-Reynolds-number conditions considered herein, the axisymmetric stream functions for flow fields inside and outside of the tangent drops satisfy (Kim & Karrila 1991):

$$\mathrm{E}^4\psi = \mathrm{E}^4\hat{\psi}_i = 0, \tag{6.1}$$

where $\hat{\psi}_i$ denotes the internal stream functions for each drop ($i = 1, 2$), ψ denotes the stream function associated with the external flow field, and $E^4\psi = E^2(E^2\psi)$ with the E^2 operator given by (5.4).

The requirements of uniform flow at infinity, vanishing normal velocities, continuous tangential velocities, and the tangential stress jump, (1.11), yield nine boundary conditions for ψ and $\hat{\psi}_i$:

$$\psi = \frac{1}{2}\left(\frac{\nu}{\eta^2+\nu^2}\right)^2 U_P \quad (\eta^2+\nu^2 \to 0), \tag{6.2}$$

$$\psi = 0 \quad (\eta = -\eta_1, +\eta_2), \tag{6.3}$$

$$\hat{\psi}_1 = 0, \quad \hat{\psi}_2 = 0 \quad (\eta = -\eta_1, +\eta_2), \tag{6.4}$$

$$\frac{\partial\psi}{\partial\eta} = \frac{\partial\hat{\psi}_1}{\partial\eta}, \quad \frac{\partial\psi}{\partial\eta} = \frac{\partial\hat{\psi}_2}{\partial\eta} \quad (\eta = -\eta_1, +\eta_2), \tag{6.5}$$

$$\hat{\sigma}_{\eta\nu} - \sigma_{\eta\nu} = \beta(\nabla T)_\nu \quad (\eta = -\eta_1, +\eta_2), \tag{6.6}$$

where η_1 and η_2 define the drop surfaces according to (5.2), U_P is the pairwise migration velocity of the tangent drops, $\beta = -\partial\gamma/\partial T$ is the variation of interfacial tension with temperature, and $(\nabla T)_\nu$ is the tangential temperature gradient on the drop surfaces given by (5.16) and (5.17) for non-conducting drops. The tangential traction on the drop surfaces, $\sigma_{\eta\nu}$ and $\hat{\sigma}_{\eta\nu,i}$, are (Reed & Morrison 1974):

$$\sigma_{\eta\nu} = -\mu\frac{1}{\nu}(\eta^2+\nu^2)^{\frac{3}{2}}\frac{\partial^2}{\partial\eta^2}[(\eta^2+\nu^2)^{\frac{3}{2}}\psi], \tag{6.7}$$

$$\hat{\sigma}_{\eta\nu,i} = -\lambda\mu\frac{1}{\nu}(\eta^2+\nu^2)^{\frac{3}{2}}\frac{\partial^2}{\partial\eta^2}[(\eta^2+\nu^2)^{\frac{3}{2}}\hat{\psi}_i]. \tag{6.8}$$

If $E^2\psi^* = 0$, then $\psi = z\psi^*$, and $\psi = r^2\psi^*$ are linearly independent solutions of (6.1). Thus, a general solution can be constructed by the superposition $\psi = c_1 z\psi^* + c_2 r^2\psi^*$, where ψ^* is given by the first term of (5.10); thus, a general, non-singular solution of (6.1) that also satisfies (6.2) is

$$\psi = \frac{\nu}{(\eta^2+\nu^2)^{\frac{3}{2}}}\int_0^\infty [(A(s)+C(s)\,\eta)\sinh s\eta + (B(s)+D(s)\,\eta)\cosh s\eta]\,J_1(s\nu)\,\mathrm{d}s + \frac{1}{2}\left(\frac{\nu}{\eta^2+\nu^2}\right)^2 U_P, \tag{6.9}$$

which can be written using an identity (Erdelyi *et al.* 1954),

$$\frac{\nu}{(\eta^2+\nu^2)^{\frac{1}{2}}} = \int_0^\infty \mathrm{e}^{-s|\eta|}\left(|\eta|+\frac{1}{s}\right)J_1(s\nu)\,\mathrm{d}s, \tag{6.10}$$

to yield

$$\psi = \frac{\nu}{(\eta^2+\nu^2)^{\frac{3}{2}}}\int_0^\infty \left[(A(s)+C(s)\,\eta)\sinh s\eta + (B(s)+D(s)\,\eta)\cosh s\eta + \tfrac{1}{2}\mathrm{e}^{-s|\eta|}\left(|\eta|+\frac{1}{s}\right)U_P\right]J_1(s\nu)\,\mathrm{d}s. \tag{6.11}$$

Noting that $-\eta_1 \geqslant \eta \geqslant -\infty$ within drop 1 and $\eta_2 \leqslant \eta \leqslant +\infty$ within drop 2, non-singular stream functions that describe the internal flow fields are given by

$$\hat{\psi}_1 = \frac{\nu}{(\eta^2+\nu^2)^{\frac{5}{2}}} \int_0^\infty [E(s)+F(s)\,\eta]\,\mathrm{e}^{s\eta} J_1(s\nu)\,\mathrm{d}s, \tag{6.12}$$

$$\hat{\psi}_2 = \frac{\nu}{(\eta^2+\nu^2)^{\frac{5}{2}}} \int_0^\infty [G(s)+H(s)\,\eta]\,\mathrm{e}^{-s\eta} J_1(s\nu)\,\mathrm{d}s. \tag{6.13}$$

The unknown functions, $A(s)$–$H(s)$, are determined from the eight boundary conditions on the drop surfaces. Inserting the stream-function expressions (6.11)–(6.13) into boundary conditions (6.3)–(6.6) yields eight algebraic equations that determine $A(s)$–$H(s)$. From (6.4),

$$E(s)-\eta_1 F(s) = 0, \tag{6.14}$$

$$G(s)+\eta_2 H(s) = 0, \tag{6.15}$$

and so $E(s)$ and $G(s)$ are easily eliminated from the system of equations. The remaining six algebraic equations are

$$-A(s)\sinh s\eta_1 + B(s)\cosh s\eta_1 + C(s)\,\eta_1 \sinh s\eta_1 - D(s)\,\eta_1 \cosh s\eta_1 = -\tfrac{1}{2}\mathrm{e}^{-s\eta_1}\left(\eta_1+\frac{1}{s}\right) U_P, \tag{6.16}$$

$$A(s)\sinh s\eta_2 + B(s)\cosh s\eta_2 + C(s)\,\eta_2 \sinh s\eta_2 + D(s)\,\eta_2 \cosh s\eta_2 = -\tfrac{1}{2}\mathrm{e}^{-s\eta_2}\left(\eta_2+\frac{1}{s}\right) U_P, \tag{6.17}$$

$$\begin{aligned} &-sA(s)\cosh s\eta_1 + sB(s)\sinh s\eta_1 + C(s)(s\eta_1\cosh s\eta_1 + \sinh s\eta_1) \\ &-D(s)(s\eta_1\sinh s\eta_1 + \cosh s\eta_1) + F(s)\,\mathrm{e}^{-s\eta_1} = \tfrac{1}{2}s\eta_1\,\mathrm{e}^{-s\eta_1} U_P, \end{aligned} \tag{6.18}$$

$$\begin{aligned} &-sA(s)\cosh s\eta_2 - sB(s)\sinh s\eta_2 - C(s)(s\eta_2\cosh s\eta_2 + \sinh s\eta_2) \\ &-D(s)(s\eta_2\sinh s\eta_2 + \cosh s\eta_2) + H(s)\,\mathrm{e}^{-s\eta_2} = -\tfrac{1}{2}s\eta_2\,\mathrm{e}^{-s\eta_2} U_P, \end{aligned} \tag{6.19}$$

$$\begin{aligned} &sA(s)\sinh s\eta_1 - sB(s)\cosh s\eta_1 - C(s)(2\cosh s\eta_1 + s\eta_1\sinh s\eta_1) + D(s)(2\sinh s\eta_1 \\ &+s\eta_1\cosh s\eta_1) + 2\lambda F(s)\,\mathrm{e}^{-s\eta_1} = \tfrac{1}{2}\mathrm{e}^{-s\eta_1}(s\eta_1-1)\,U_P - \frac{s\sinh s\eta_2}{\sinh s(\eta_1+\eta_2)}\frac{\beta}{\mu}\nabla T_\infty, \end{aligned} \tag{6.20}$$

$$\begin{aligned} &-sA(s)\sinh s\eta_2 - sB(s)\cosh s\eta_2 - C(s)(2\cosh s\eta_2 + s\eta_2\sinh s\eta_2) - D(s)(2\sinh s\eta_2 \\ &+s\eta_2\cosh s\eta_2) - 2\lambda H(s)\,\mathrm{e}^{-s\eta_2} = \tfrac{1}{2}\mathrm{e}^{-s\eta_2}(s\eta_2-1)\,U_P - \frac{s\sinh s\eta_1}{\sinh s(\eta_1+\eta_2)}\frac{\beta}{\mu}\nabla T_\infty. \end{aligned} \tag{6.21}$$

Unlike the solution for the temperature field, given by (5.10) and (5.15), a closed-form solution for the velocity stream function is impractical. An exception is the special case of equisized drops, which is of limited interest herein because they migrate with equal velocity.

The forces acting on the drops are (Reed & Morrison 1974):

$$F_1 = 4\pi\int_0^\infty s[A(s)-B(s)]\,\mathrm{d}s, \quad F_2 = -4\pi\int_0^\infty s[A(s)+B(s)]\,\mathrm{d}s. \tag{6.22}$$

These expressions are numerically integrated on a set of quadrature points. Taking $U_p = 1$ and $\beta\nabla\mathrm{T}_\infty = 0$ gives $R_i^H = F_i$, conversely, setting $U_P = 0$ and $\beta\nabla T_\infty = 1$ yields

$R_i^T = F_i$. The results of Reed & Morrison (1974) are recovered by the first choice; the latter choice yields the desired forces on a pair of non-conducting, stationary, tangent drops aligned with an ambient temperature gradient, ∇T_∞.

The buoyancy-driven and thermocapillary-driven pair and individual drop velocities and contact forces are obtained by inserting the pairwise resistances, R_i^H and R_i^T, and the formulae for the lubrication resistance, R_{12}^H, into the expressions derived in §2. Numerical results are presented in the §7.

6.2. *Velocity field near the contact point*

The validity of (2.9) and (2.10) requires an analysis of the velocity field in the lubrication gap between the drops. The requisite analysis of the velocity field for two drops in buoyancy-driven motion is available from previous work by Yiantsios & Davis (1991). In this section, we summarize this analysis and then generalize it to include thermocapillary-driven motion.

Yiantsios & Davis (1991) demonstrated that the primary velocity field associated with axisymmetric, pairwise translation of drops in near contact decays algebraically in the near-contact region:

$$u/U_P^G = O(\rho/\alpha) \quad (\rho = O(\alpha\epsilon^{\frac{1}{2}})). \tag{6.23}$$

It follows that the resultant hydrodynamic stress acting on the near-contact region from the primary, buoyancy-driven velocity field makes an $O(\epsilon^{\frac{3}{2}})$ contribution to the general hydrodynamic resistance functions, A_{11}^H and A_{21}^H, defined by (2.1). The velocity field away from the gap is obtained to $O(\epsilon)$ by considering a pair of drops in point contact. Thus, (2.9) is correct as asserted. Yiantsios & Davis (1991) give scaling arguments that demonstrate that the lubrication flow dominates the primary, buoyancy-driven velocity field in the near-contact region provided that the drops are not almost equisized ($1-\kappa \gg \epsilon^{\frac{1}{2}}$). Since the lubrication flow dominates the primary, buoyancy-driven velocity field in the near-contact region, the flow fields may be decoupled in the gap region, which is advantageous when local droplet deformation becomes significant.

In thermocapillary-driven flows, fluid is driven by interfacial tension gradients that may affect the fluid velocity in the gap region. The interfacial tension gradients is proportional to the tangential component of the temperature gradient on the drop surfaces: $(\nabla\gamma)_s = \beta(\nabla T)_s$; thus, using (5.26) we find that interfacial tension gradients are exponentially small in the gap region and therefore insignificant. The primary thermocapillary-driven velocity field in the near-contact region can therefore be reliably estimated using (6.23) with the pairwise velocity given by U_P^T instead of U_P^G. It follows that the velocity field in the gap region affects the thermocapillary resistance functions, A_1^T and A_2^T, at $O(\epsilon^{\frac{3}{2}})$; the $O(\epsilon)$ contributions to the temperature and velocity field away from the gap of two slightly separated drops dominate; thus, (2.10) is justified. The same scaling arguments given by Yiantsios & Davis (1991) apply with the same result: lubrication flow dominates the primary, thermocapillary-driven flow in the near-contact region provided $\epsilon^{\frac{1}{2}} \ll 1-\kappa$. To leading order, the lubrication flow that results from the nearly constant contact force, F_{12}, is the same for buoyancy-driven and thermocapillary-driven motion.

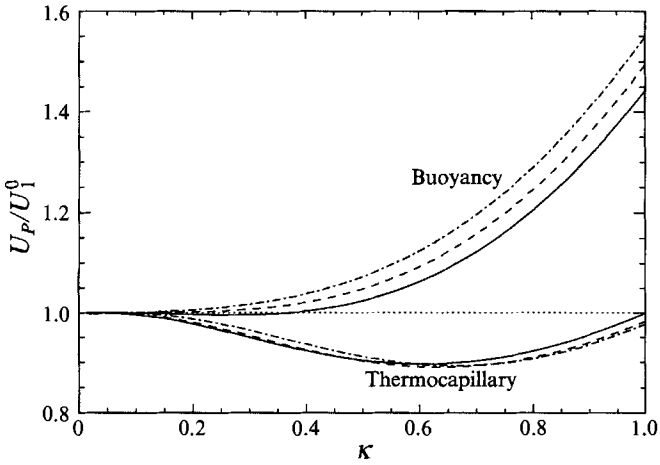

FIGURE 3. Thermocapillary and buoyancy pair migration velocities normalized by the isolated migration velocity of the larger drop; the solid lines are for $\lambda = 0$, the dashed lines are for $\lambda = 1$, and the dashed-dotted lines are for $\lambda \to \infty$.

7. Numerical results and discussion

7.1. *Pairwise migration velocity*

Figure 3 shows the axisymmetric, buoyancy-driven and thermocapillary-driven pairwise migration velocity, normalized by the isolated migration velocity of the larger drop. Because of this normalization, parameters such as β, ∇T_∞, $\Delta\rho$, and g do not appear in the dimensionless results presented, whereas the dimensional results for the drop velocities are proportional to these parameters because of the linearity of the governing equations. Results for $\lambda = 0$ (bubbles), $\lambda = 1$, and $\lambda \to \infty$ are shown. For buoyancy motion, $\lambda \to \infty$ describes the sedimentation of rigid particles; for thermocapillary migration, it describes the limiting case for highly viscous drops (rigid particles do not undergo thermocapillary migration). To within 1%, the limiting result, $\lambda \to \infty$, is obtained for $\lambda \geqslant 100$. The buoyancy results agree with those of Reed & Morrison (1974).

In contrast to the scaling result for buoyancy motion, (4.3) does not predict whether the thermocapillary velocity of a pair of equal drops ($\kappa = 1$), U_{EQ}^T, is greater or less than that of a single drop, $U_1^{T,0}$, because both the thermocapillary driving force and the viscous opposing force on each drop are reduced by the pairwise configuration. In fact, the results depicted in figure 3 indicate that equisized bubbles undergo pairwise, thermocapillary migration with the same velocity as an isolated bubble, which is consistent with earlier results for equisized bubbles (Feuillebois 1989; Acrovis, Jeffrey & Saville 1990); for $\lambda \neq 0$, U_{EQ}^T is only slightly less than $U_1^{T,0}$. The buoyancy-driven, pairwise migration velocity of equisized drops exceeds the isolated drop velocity by 44% for bubbles ($\lambda = 0$) and by 55% for rigid particles ($\lambda \to \infty$) and $1.44 < U_{EQ}^G/U_1^{G,0} < 1.55$ for $\lambda = O(1)$ which is consistent with (4.3).

The results depicted in figure 3 indicate that the buoyancy-driven doublet velocity exceeds the singlet velocity ($U_P^G > U_1^{G,0}$) for almost all κ and λ. The enhancement increases monotonically with λ and κ, except for $\lambda = 0$, $\kappa \leqslant 0.25$. For $\lambda = 0$ and $\kappa < 0.37$, the buoyancy-driven, pair migration velocity apparently lags slightly ($< 0.5\%$) behind $U_1^{G,0}$. In contrast, the thermocapillary-driven doublet velocity obeys $U_P^T < U_1^{T,0}$ for all λ and κ. To within 3%, the value of $U_P^T/U_1^{T,0}$ is insensitive to λ; for $\kappa > 0.6$, the value of $U_P^T/U_1^{T,0}$ decreases slightly with λ; the trend reverses for

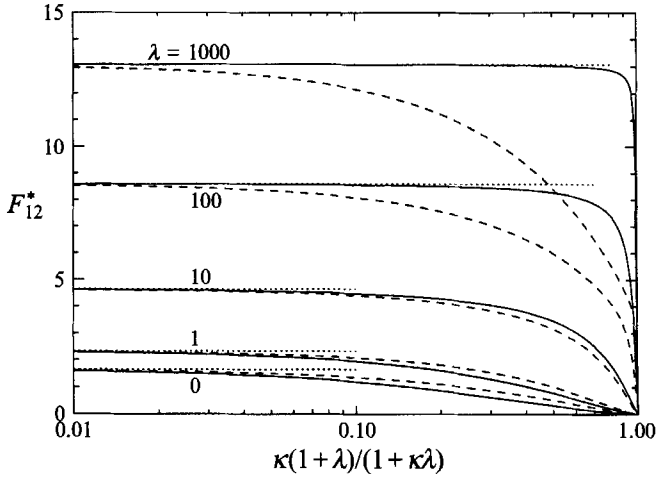

FIGURE 4. Normalized (according to (7.1)) contact force between two drops; the solid line is for thermocapillary motion, the dashed line is for buoyancy motion, and the dotted line is for $\kappa \to 0$.

$\kappa < 0.5$. At $\kappa \approx 0.6$, the value of $U_P^T/U_1^{T,0}$ attains a minimum value of 0.88. For nearly equisized drops, U_P appears to decrease linearly with $1-\kappa$, consistent with (4.2); furthermore, the results appear consistent with (4.4) for $\kappa \to 0$.

7.2. *Contact force*

Figure 4 depicts the scaled, buoyancy (dashed curves) and thermocapillary (solid curves) contact forces between drops undergoing axisymmetric motion for several viscosity ratios; dotted curves correspond to the $\kappa \to 0$ limit. The contact force has been made dimensionless by rescaling as

$$F_{12}^{G*} = \frac{1}{\kappa^2}\frac{\lambda+1}{\kappa\lambda+1}\frac{F_{12}^G}{F_1^G}, \quad F_{12}^{T*} = \frac{1}{3\kappa^2}\frac{F_{12}^T}{F_1^{T,0}}, \tag{7.1}$$

where F_1^G and $F_1^{T,0}$ are the buoyancy and thermocapillary (isolated drop) forces acting on the larger drop, respectively, given by (1.2) and (1.5). This choice of normalization is consistent with the scaling results, (4.8) and (4.10), for $\kappa \ll 1$, and the asymptotic result, (4.15), for $\kappa(\lambda+1) \ll 1$. For nearly equal drops ($1-\kappa \ll 1$), we note that $1-\kappa(1+\lambda)/(1+\kappa\lambda) \approx (1-\kappa)/(1+\lambda)$, and the results near the right-hand side of figure 4 are seen to verify the scaling result, (4.1).

7.2.1. *Small size ratios:* $\kappa \ll 1$

When $\kappa \ll 1$ and $\kappa\lambda \ll 1$, the asymptotic formula, (4.15), predicts that $F_{12}^{T*} = F_{12}^{G*}$. This result is verified by figure 4. The limiting contact force for $\kappa \to 0$ is depicted by the solid curve in figure 5. These numerical results apparently tend to the dotted lines that have the formulae

$$F_{12}^{G*} = F_{12}^{T*} = \pi^2/6 \quad (\lambda \ll 1); \qquad F_{12}^{G*} = F_{12}^{T*} = 2\ln\lambda - \tfrac{3}{4} \quad (\lambda \gg 1). \tag{7.2}$$

Analytical derivations for these results were not found. To within 2%, the numerical results for all λ are represented by

$$F_{12}^{G*} = F_{12}^{T*} = \frac{2\lambda\ln(\lambda+28) - \frac{3}{4}\lambda + 10}{\lambda+6} \quad (\kappa \ll 1). \tag{7.3}$$

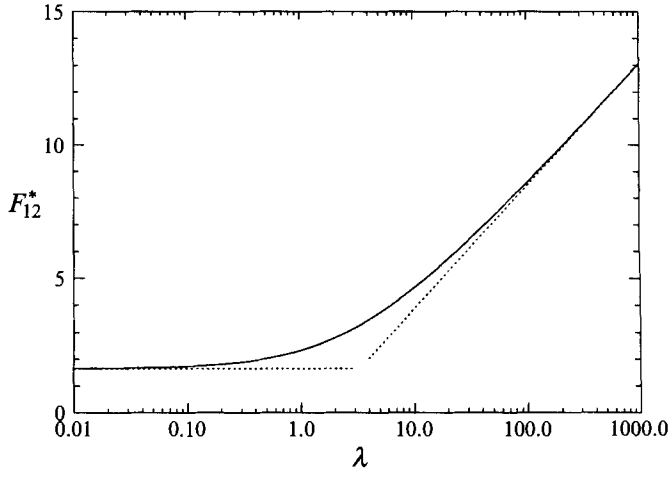

FIGURE 5. Normalized (according to (7.1)) contact force between two drops; the solid line is the limiting result for $\kappa \to 0$, the dotted lines are the limiting results: $F_{12}^* = \pi^2/6$, and $F_{12}^* = 2\ln\lambda - \frac{3}{4}$ obtained for $\lambda \ll 1$ and $\lambda \gg 1$, respectively.

Combining this formula with the rescalings, (7.1), yields

$$\frac{R_2^H}{R_1^{H,0}} = \frac{F_{12}^G}{F_1^G} = \kappa^2 \frac{2\lambda \ln(\lambda+28) - \frac{3}{4}\lambda + 10}{(\lambda+6)(\lambda+1)} \quad (\kappa \ll 1, \quad \kappa\lambda \ll 1), \tag{7.4}$$

$$\frac{F_{12}^T}{F_1^{T,0}} = 3\kappa^2 \frac{2\lambda \ln(\lambda+28) - \frac{3}{4}\lambda + 10}{\lambda+6} \quad (\kappa \ll 1). \tag{7.5}$$

The first equality in (7.4) follows from (2.5) and (4.4) and gives the hydrodynamic resistance of the smaller drop in near contact with a larger drop. The complement of (7.4) was computed by Goren (1970) for rigid spheres:

$$R_2^H/R_1^{H,0} = 4.844\kappa^3, \quad F_{12}^G/F_1^G = 3.844\kappa^3 \quad (\kappa \ll 1, \quad \lambda\kappa \gg 1). \tag{7.6}$$

Combining this with (7.5) gives the formula complementary to (4.15):

$$\frac{F_{12}^T}{F_{12}^G} = \frac{U_{12}^T}{U_{12}^G} = 1.561\kappa^{-1}(\ln\lambda - \tfrac{3}{8})\frac{U_1^{T,0}}{U_1^{G,0}} \quad (\kappa \ll 1, \quad \kappa\lambda \gg 1). \tag{7.7}$$

7.3. *Relative drop velocity*

7.3.1. *Asymptotic formulae for* $\kappa \ll 1$

According to (2.13), the asymptotic formulae (7.4)–(7.6) for F_{12} may be combined with (3.3)–(3.5) for the lubrication resistance to yield the asymptotic formulae:

$$\frac{U_{12}^G}{U_1^{G,0}} = \kappa\left(\frac{\lambda+\frac{2}{3}}{\lambda+1}\right)\frac{2\lambda\ln(\lambda+28) - \frac{3}{4}\lambda + 10}{(\lambda+6)(\lambda+1)}F(\epsilon,\lambda) \quad (\kappa \ll 1, \quad \kappa\lambda \ll 1), \tag{7.8}$$

$$\frac{U_{12}^G}{U_1^{G,0}} = 3.844\kappa^2 F(\epsilon,\lambda) \quad (\kappa \ll 1, \quad \kappa\lambda \gg 1), \tag{7.9}$$

$$\frac{U_{12}^T}{U_1^{T,0}} = 3\kappa\left(\frac{\lambda+\frac{2}{3}}{\lambda+1}\right)\frac{2\lambda\ln(\lambda+28) - \frac{3}{4}\lambda + 10}{\lambda+6}F(\epsilon,\lambda) \quad (\kappa \ll 1), \tag{7.10}$$

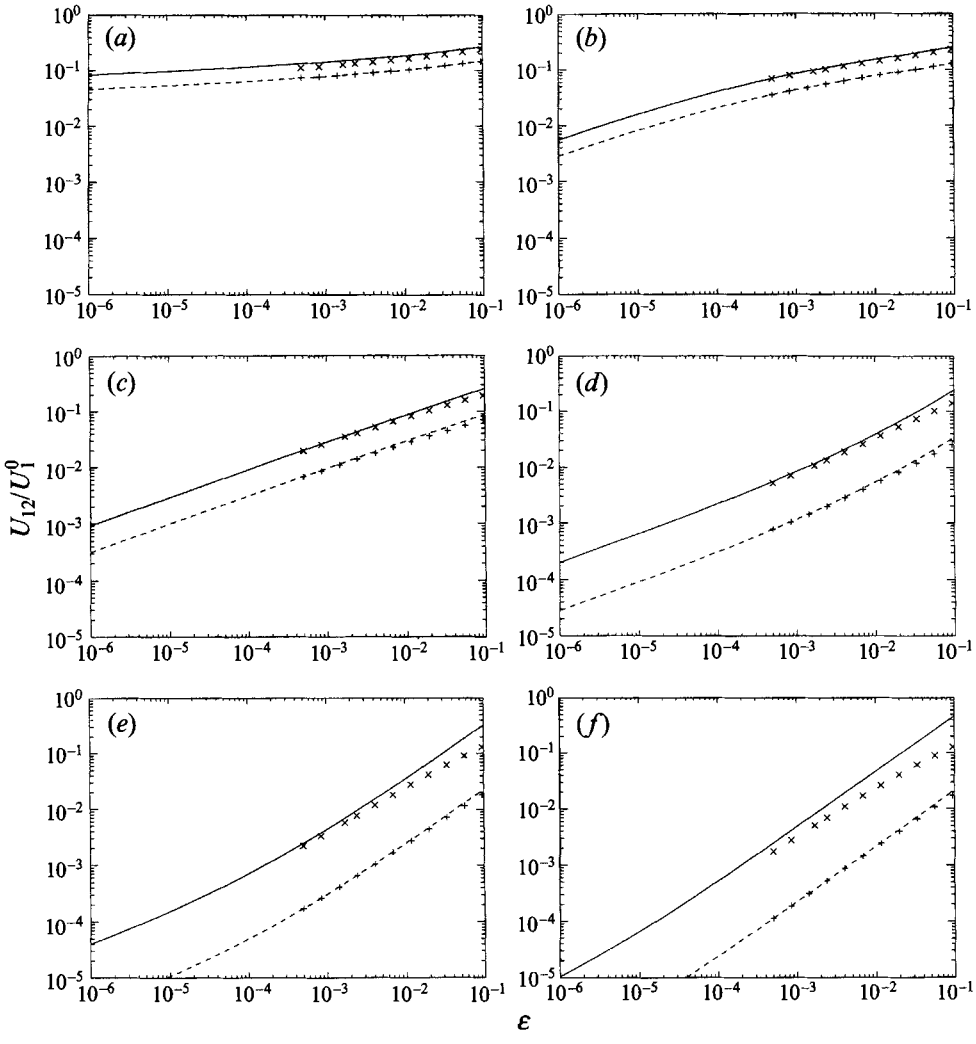

FIGURE 6. Thermocapillary-driven (solid lines) and buoyancy-driven (dashed lines) relative drop velocities normalized by the isolated migration velocity of the larger drop for a size ratio of $\kappa = 0.5$; the symbols are from exact bispherical coordinate solutions. (*a*) $\lambda = 0$; (*b*) $\lambda = 0.1$; (*c*) $\lambda = 1$; (*d*) $\lambda = 10$; (*e*) $\lambda = 100$; (*f*) $\lambda = 1000$.

where
$$F(\epsilon, \lambda) = \epsilon \qquad (\lambda \epsilon^{\frac{1}{2}} \gg 1), \tag{7.11}$$

$$F(\epsilon, \lambda) = \frac{16}{\pi^2} \lambda^{-1} (\tfrac{1}{2}\epsilon)^{\frac{1}{2}} \qquad (1 \gg \lambda \epsilon^{\frac{1}{2}} \gg \epsilon \ln \epsilon^{-1}), \tag{7.12}$$

$$F(\epsilon, \lambda) = 3[\ln 2\epsilon^{-1} + 2\gamma_E]^{-1} \qquad (\lambda \epsilon^{\frac{1}{2}} \ll \epsilon \ln \epsilon^{-1}). \tag{7.13}$$

7.3.2. *Numerical results*

Figure 6 depicts the buoyancy-driven (dashed curves) and thermocapillary-driven (solid curves) relative drop velocities as a function of gap width for a radius ratio of $\kappa = 0.5$, with viscosity ratios of $\lambda = 0$, 0.1, 1, 10, 100, and 1000. According to (2.13), it follows that the ratio of U_{12}^G to U_{12}^T will be independent of ϵ for $\epsilon \ll 1$, because both F_{12}^G and F_{12}^T are independent of ϵ in this limit. In fact, the numerical results predict that

U_{12}^T/U_{12}^G equals 1.82, 1.95, 2.93, 7.13, 14.3, and 21.7 times $U_1^{T,0}/U_1^{G,0}$ for $\kappa = 0.5$ and $\lambda = 0$, 0.1, 1, 10, 100, and 1000, respectively. The normalized, thermocapillary-driven relative drop velocity for $\kappa = 0.5$ is significantly larger than that for buoyancy-driven motion, particularly for $\lambda > 1$, in contrast to the prediction (4.1) of comparable values for $1-\kappa \ll 1$. However, using (4.15) for $\kappa\lambda < 1$ and (7.7) for $\kappa\lambda > 1$, yields good estimates: $U_{12}^T/U_{12}^G = 3$, 3.3, 6, 6.02, 13.2, and 20.4 times $U_1^{T,0}/U_1^{G,0}$ for $\kappa = 0.5$ and $\lambda = 0$, 0.1, 1, 10, 100, and 1000, respectively.

It is interesting to note from figure 6 several manifestations of the distinct limiting forms of the lubrication resistance, (3.3)–(3.5). For $\lambda = 0$, the relative velocity exhibits the $1/\ln\epsilon^{-1}$ dependence characteristic of free surfaces; this behaviour is again evident for $\lambda = 0.1$ for $\epsilon > 10^{-3}$, where $\lambda\epsilon^{\frac{1}{2}} < \epsilon\ln\epsilon^{-1}$, but the dependence switches to the $\epsilon^{\frac{1}{2}}$ behaviour characteristic of a fully mobile interface for $\epsilon < 10^{-4}$, where $\lambda\epsilon^{\frac{1}{2}} > \epsilon\ln\epsilon^{-1}$. For $\lambda = 1$, the fully mobile behaviour is evident over the entire range of ϵ, which follows since $\epsilon\ln\epsilon^{-1} \ll \lambda\epsilon^{\frac{1}{2}} \ll 1$ under these conditions. For $\lambda = 10$ and 100, the immobile ϵ-dependence is evident for $\epsilon\lambda^{\frac{1}{2}} > 1$; fully mobile behaviour is observed for smaller values of ϵ. In contrast, immobile interface behaviour is apparent for $\lambda = 1000$ for the entire range of ϵ shown; presumably, the interface would become fully mobile for $\epsilon < 10^{-6}$, where $\lambda\epsilon^{\frac{1}{2}} < 1$.

The results of the lubrication calculations depicted in figure 6 were compared with the exact, bispherical-coordinate solutions (calculated on our computer) of Zinchenko (1978) and Keh & Chen (1990), as indicated by the + and × symbols for buoyancy-driven and thermocapillary-driven motion, respectively. Calculations using the authors' FORTRAN algorithm compiled on our computer for $\epsilon \leqslant 2.25\times10^{-4}$ showed essentially exact agreement with the lubrication solution for buoyancy-driven motion, whereas numerical convergence of calculations for thermocapillary-driven motion was not obtained for $\epsilon \leqslant 2.25\times10^{-4}$. The published results of Keh & Chen (1990) are restricted to $\epsilon \geqslant 0.03$. For buoyancy motion, the results indicate that the exact solution tends to the lubrication solution for $\epsilon\to0$; convergence appears to be slowest for $\lambda = 0(1)$. By contrast, the exact thermocapillary solution tends much more slowly to the lubrication solution, and the rate of convergence is slowest for $\lambda \gg 1$. An exception to this trend occurs for $\lambda = 0$; in this case, convergence is not apparent. The source of the discrepancy is unclear but may be related to the computational difficulties encountered using the exact, bispherical coordinate solution for small gap widths ($\epsilon \leqslant 2.25\times10^{-4}$. The exact numerical results of Satrape (1992) and Meyyappan, Wilcox & Subramanian (1983) for bubbles ($\lambda = 0$) are, unfortunately, restricted to $\epsilon \geqslant 0.02$ and $\epsilon \geqslant 0.31$, respectively.

7.4. *Individual drop velocities*

7.4.1. *Numerical results*

Figure 7 depicts the individual drop velocities for $\epsilon = 10^{-2}$ and 10^{-4}, and $\lambda = 0$, 0.1, 1, 10, 100, and 1000; the results are normalized by U_1^0. Solid curves depict the pair velocity, U_P, which is attained by both drops in the limit $\epsilon\to0$ (see figure 3); the dashed curves depict U_1, which exceeds U_P, and the dashed-dotted curves depict U_2, which lags U_P. Inspection of figure 7 reveals that, for $1-\kappa \ll 1$, $U_1-U_P \approx U_P-U_2$ and the deviations appear to grow linearly with $1-\kappa$, consistent with the scaling predictions (4.2). In contrast with (4.2), however, the thermocapillary-driven, deviation velocities appear to be significantly larger than those for buoyancy-driven motion, especially for $\lambda \gg 1$. A comparison of figures 7(*a*) and 7(*g*), 7(*b*) and 7(*h*), 7(*c*) and 7(*i*), and 7(*d*) and 7(*j*) exemplifies how U_{12} vanishes as $\epsilon\to0$ for fixed λ. The very slow, logarithmic decay for $\epsilon\lambda^{\frac{1}{2}} \ll \epsilon\ln\epsilon^{-1}$ is most apparent for $\lambda = 0$; as figures 7(*b*) and 7(*h*) illustrate,

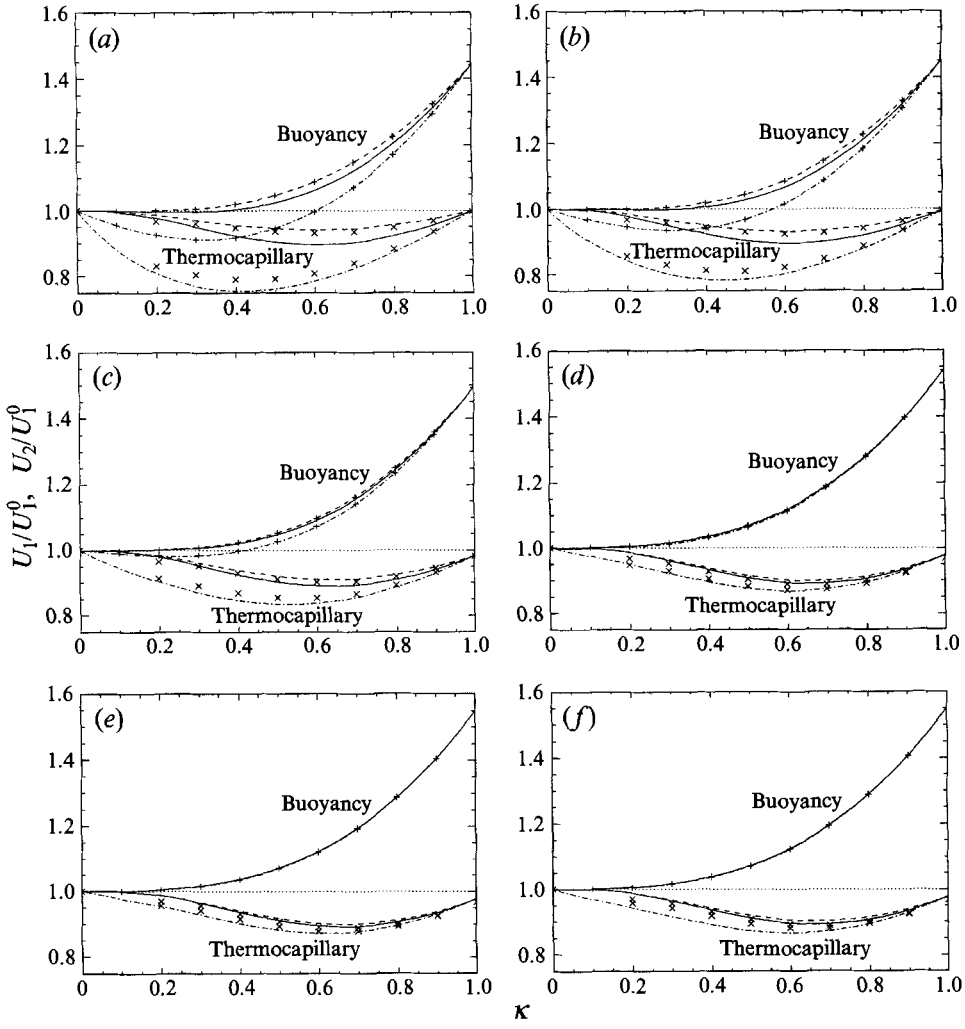

FIGURE 7(*a–f*). For caption see facing page.

even slight drop viscosity ($\lambda = 0.1$) significantly retards U_{12} as ϵ is decreased. This observation is explained by (7.12) and (7.13): free and fully mobile interfaces exhibit qualitatively different behaviour as demonstrated by figure 6 for $\lambda = 0$ and 0.1.

The progression depicted in figure 7(*a–f*) for $\epsilon = 10^{-2}$ indicates that U_{12} is reduced as the viscosity ratio, λ, is increased; however, the reduction is much more pronounced for buoyancy-driven motion. For $\epsilon = 10^{-2}$, the results indicate that $U_{12}^G \leqslant 0.005 U_1^{G,0}$ for $\lambda \geqslant 10$; for the same gap width, U_{12}^T decreases with increasing λ for $\lambda \leqslant 10$ ($U_{12}^T \leqslant 0.04 U_1^{T,0}$ for $\lambda = 10$); however, U_{12}^T increases slightly with increasing λ in the range $10 \leqslant \lambda \leqslant 1000$ ($U_{12}^T \leqslant 0.05 U_1^{T,0}$ for $\lambda = 1000$). The latter observation is predicted by the asymptotic formulae (7.10) and (7.13) that were derived for $\kappa \ll 1$; accordingly, $U_{12}^T = O(\kappa\epsilon \ln \lambda)$ for $\lambda > O(\epsilon^{-\frac{1}{2}})$. This regime is not attained in the progression depicted by figure 7(*g–j*) for $\epsilon = 10^{-4}$.

The + and × symbols in figure 7 for $\epsilon = 10^{-2}$ are from exact bispherical-coordinate calculations for buoyancy and thermocapillary migration using the source code of Zinchenko (1978) and Keh & Chen (1990). Note that the present lubrication results for

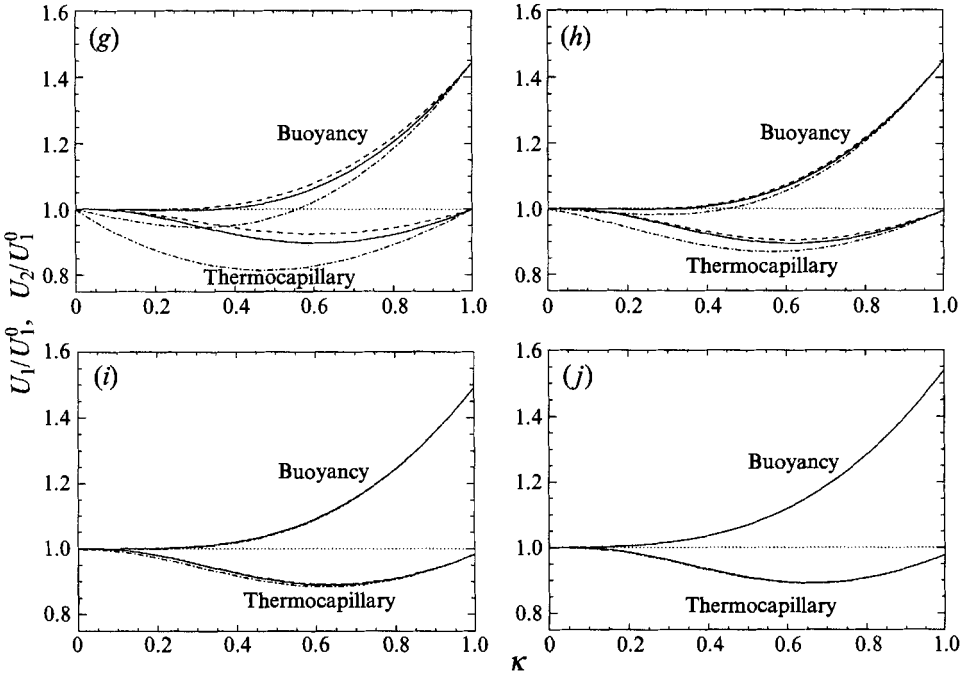

FIGURE 7. Individual drop velocities, normalized by the isolated migration velocity of the larger drop, for two drops in close contact; the solid line is the pairwise velocity of touching drops, the dashed line is the velocity of the larger drop, and the dotted-dashed line is for the smaller drop. (*a*) $\lambda = 0$; (*b*) $\lambda = 0.1$; (*c*) $\lambda = 1$; (*d*) $\lambda = 10$; (*e*) $\lambda = 100$; (*f*) $\lambda = 1000$; (*g*) $\lambda = 0$; (*h*) $\lambda = 0.1$; (*i*) $\lambda = 1$; (*j*) $\lambda = 10$. (*a–f*) $\epsilon = 10^{-2}$; (*h–j*) $\epsilon = 10^{-4}$.

the thermocapillary-driven motion of each drop are less accurate than those for buoyancy-driven motion, particularly for $\lambda \gg 1$ which is consistent with figure 6. For $\epsilon = 10^{-4}$, essentially exact agreement was obtained for buoyancy motion. Bispherical-coordinate calculations for thermocapillary migration were not possible for $\epsilon = 10^{-4}$ because of the lack of numerical convergence.

7.4.2. *Small size ratios:* $\kappa \ll 1$

The individual drop velocities are generally given by (2.11). From (4.7), (7.4), and (7.6), we have, at leading order

$$\frac{U_P - U_2}{U_{12}} = 1 \qquad (\kappa \ll 1), \tag{7.14}$$

$$\frac{U_1 - U_P}{U_{12}} = \kappa^2 \frac{2\lambda \ln(\lambda+28) - \frac{3}{4}\lambda + 10}{(\lambda+6)(\lambda+1)} \qquad (\kappa \ll 1, \quad \kappa\lambda \ll 1), \tag{7.15}$$

$$\frac{U_1 - U_P}{U_{12}} = 4.844\kappa^3 \qquad (\kappa \ll 1, \quad \kappa\lambda \gg 1), \tag{7.16}$$

where U_{12} is given by (7.8)–(7.10). These results predict that $U_P^T - U_2^T$ vanishes linearly as $\kappa \to 0$; the same is true for $U_P^G - U_2^G$ if $\kappa\lambda \ll 1$; for $\kappa\lambda \gg 1$, the formulae predict that $U_P^G - U_2^G \to 0$ as κ^2. For both migration mechanisms, $U_1 - U_P \to 0$ as κ^2 if $\kappa\lambda \ll 1$, otherwise faster. Each of these observations is qualitatively apparent in figure 7, particularly, the linear behaviour of $U_P - U_2$ for $\kappa \ll 1$.

7.5. *Discussion*

During thermocapillary migration, a drop 'swims' through the suspending phase as a result of an interfacial tension gradient that convects surrounding fluid along the drop surface from the forward to the rear stagnation point. The drop is propelled in the direction opposite to the momentum of the convected fluid. This contrasts with the mechanism of buoyancy-driven migration in which surrounding fluid is only passively convected past the drop surface as the result of a body force. In both buoyancy-driven and thermocapillary-driven near-contact motion of a pair of drops, continuous-phase fluid must be forced out of the lubrication gap as the larger drop approaches the smaller drop. The thermocapillary-driven approach is enhanced by the *withdrawal* of fluid from the lubrication gap as a result of fluid convection along the larger drop surface. This is partially offset by the *injection* of fluid into the lubrication gap resulting from convection along the surface of the smaller drop. For $\kappa \ll 1$, the withdrawal of fluid by the larger drop easily dominates the injection from the smaller drop, consistent with (4.15) and (7.7) which predict that the thermocapillary-driven approach is more effective than the buoyancy-driven approach.

The qualitative agreement between the predictions of the asymptotic formulae derived for $\kappa \ll 1$ and the numerical results depicted in figures 6 and 7 suggest that the asymptotic behaviour for $\kappa \to 0$ pervades to finite κ. In fact, it seems likely that the withdrawal of fluid from the lubrication gap by the larger drop should dominate the injection from the smaller drop except when the drops are nearly equisized ($1-\kappa \ll 1$). Only for nearly equal drops will the withdrawal and injection of continuous-phase fluid be approximately balanced and only then will near-contact thermocapillary motion be qualitatively similar to buoyancy-driven motion. Thus, the scaling results for nearly equisized drops have a rather limited domain of validity ($\kappa \geqslant 0.9$), while the asymptotic formulae for $\kappa \ll 1$ are qualitatively correct even for $\kappa = 0.5$ or larger.

8. Concluding remarks

In this work, we have computed the axisymmetric, near-contact thermocapillary motion of a pair of non-conducting drops. An analogy with buoyancy-driven droplet migration is revealed. Both mechanisms involve a superposition of a pairwise migration and a secondary, relative motion of the drops that results from a constant interdroplet, contact force balanced by a lubrication resistance.

For very nearly equisized drops, a scaling analysis predicts qualitatively similar behaviour for both buoyancy-driven and thermocapillary-driven near-contact motion; the relative velocity between widely separated drops yields a criterion, (1.6), that reliably estimates the importance of buoyancy-driven and thermocapillary-driven contributions to the relative near-contact drop velocity. However, for small size ratios ($\kappa \ll 1$), the scaling analysis predicts distinct, qualitative differences for the two mechanisms of droplet motion. Most importantly, the simple criterion, (1.6), will always underestimate the importance of the thermocapillary contribution to the relative drop velocity for $\kappa \ll 1$; for large viscosity ratios ($\lambda \gg 1$), the thermocapillary contribution will be much larger than predicted by (1.6).

Numerically results for the pairwise migration velocity, contact force, and the relative and individual drop velocities are presented for a wide range of viscosity and size ratios. The scaling predictions for $\kappa \ll 1$ are quantified with asymptotic formulae for the contact force and the relative and individual drop migration velocities. Scaling predictions for $1-\kappa \ll 1$ are qualitatively observed in a limited region: $\kappa \geqslant 0.9$.

However, many qualitative predictions for $\kappa \ll 1$ are clearly manifest for $\kappa = O(1)$. In particular, the ratio of the thermocapillary-driven to buoyancy-driven relative drop velocities, depicted in figures 6 and 7, qualitatively obeys the asymptotic formulae (7.8)–(7.10) for all size ratios. This finding disqualifies (1.6) as a valid estimate for the importance of thermocapillary and buoyancy contributions to the near-contact relative drop velocity in polydisperse emulsions. A qualitative explanation for these findings was put forth in §7.5.

The results depicted in figure 6 and the computational difficulties encountered with an exact series solution for thermocapillary migration at small gap widths suggest that the lubrication solution formulated herein will be particularly useful for obtaining accurate predictions of the thermocapillary-driven relative velocity of drops in close contact, such as are needed for calculating coalescence rates. In obtaining this solution, a new analytical result, given by (5.10) and (5.15), was obtained for the axisymmetric temperature field around an unequal pair of non-conducting, tangent spheres embedded in an ambient temperature gradient. A new asymptotic result, given by (7.4), was also obtained for the hydrodynamic resistance on a very small drop ($\kappa \ll 1, \kappa\lambda \ll 1$) tangent to a much larger, translating drop; this complements the earlier result of Goren (1970) for rigid particles and very viscous drops ($\kappa \ll 1, \kappa\lambda \gg 1$).

We conclude by noting that lubrication forces will cause the drops to deform slightly in the region of near contact. An estimate of the deformation is F_{12}/γ, and so the deformation is small compared to the gap width only so long as $F_{12}/\alpha\gamma\epsilon \ll 1$. This criterion may be met for a small initial separation, but it will eventualy be violated as $\epsilon \to 0$. Fortunately, the pairwise migration velocity and contact force are unaffected to leading order by the details of the near-contact region, for both thermocapillary-driven and gravity-driven motion, provided that in the former case the thermal conductivity of the drops is small relative to that of the continuous phase. Thus, the analysis of Yiantsios & Davis (1990, 1991) for the time evolution of the relative drop velocity and near-contact deformation for buoyancy-driven motion may be directly extended to thermocapillary-driven motion of non-conducting drops.

This work was supported by NSF grant CTS-8914236 and NASA grant NAG3-1277. The authors are grateful to Dr A. Zinchenko and Dr H. J. Keh for providing the source code that performs their calculations, and Dr D. J. Jeffrey for useful input on the solution of the temperature field around unequal, non-conducting drops.

REFERENCES

ABRAMOWITZ, M. & STEGUN, I. A. 1972 *Handbook of Mathematical Functions*. Dover.

ACRIVOS, A., JEFFREY, D. J. & SAVILLE, D. A. 1990 Particle migration in suspensions by thermocapillary or electrophoretic motion. *J. Fluid Mech.* **212**, 95–110.

ANDERSON, J. L. 1985 Droplet interactions in thermocapillary motion. *J. Multiphase Flow* **11**, 813–824.

CARRIER, G. F., KROOK, M. & PEARSON, C. E. 1966 *Functions of a Complex Variable Theory and Technique*. McGraw-Hill.

DAVIS, R. H., SCHONBERG, J. A. & RALLISON, J. M. 1989 The lubrication force between two viscous drops. *Phys. Fluids* A **1**, 77–81.

ERDELYI, A., MAGNUS, W., OBERHETTINGER, F. & TRICOMI, F. G. 1954 *Tables of Integral Transforms*, vol. II. McGraw-Hill.

FEUILLEBOIS, F. 1989 Thermocapillary migration of two equal bubbles parallel to their line of centers. *J. Colloid Interface Sci.* **131**, 267–274.

FUENTES, Y. O., KIM, S. & JEFFREY, D. J. 1988 Mobility functions for two unequal viscous drops in Stokes flow. I. Axisymmetric motions. *Phys. Fluids* **31**, 2445–2455.

FUENTES, Y. O., KIM, S. & JEFFREY, D. J. 1989 Mobility functions for two unequal viscous drops in Stokes flow. I. Asymmetric motions. *Phys. Fluids* A **1**, 61–75.

GOREN, S. L. 1970 The normal force exerted by creeping flow on a small sphere touching a plane. *J. Fluid Mech.* **41**, 619–625.

HABER, S., HETSRONI, G. & SOLAN, A. 1973 On the low Reynolds number motion of two droplets. *Intl J. Multiphase Flow* **1**, 57–71.

HAMAKER, H. C. 1937 The London–van der Waals attraction between spherical particles. *Physica* **4**, 1058–1072.

HILL, R. & POWER, G. 1956 Extremum principles for slow viscous flow and the approximate calculation of drag. *Q. J. Mech. Appl. Maths* **9**, 313–319.

KEH, H. J. & CHEN, S. H. 1990 The axisymmetric thermocapillary motion of two fluid droplets. *Intl J. Multiphase Flow* **16**, 515–527.

KIM, S. & KARRILA, S. 1991 *Microhydrodynamics: Principles and Selected Applications*. Butterworth-Heinnemann.

LEVICH, V. 1962 *Physicochemical Hydrodynamics*. Prentice Hall.

MEYYAPPAN, M., WILCOX, W. R. & SUBRAMANIAN, R. S. 1983 The slow axisymmetric motion of two bubbles in a thermal gradient. *J. Colloid Interface Sci.* **94**, 243–257.

MOON, P. & SPENCER, D. E. 1961 *Field Theory Handbook*. Springer.

REED, L. D. & MORRISON, F. A. 1974 The slow motion of two touching fluid spheres along their line of centers. *Intl J. Multiphase Flow* **1**, 573–584.

RUSHTON, E. & DAVIES, G. A. 1973 The slow unsteady settling of two fluid spheres along their line of centers. *Appl. Sci. Res.* **28**, 37–61.

SADHAL, S. S. 1983 A note on the thermocapillary migration of a bubble normal to a plane surface. *J. Colloid Interface Sci.* **95**, 283–285.

SATRAPE, J. V. 1992 Interactions and collisions of bubbles in thermocapillary motion. *Phys. Fluids* A **4**, 1883–1900.

YIANTSIOS, S. G. & DAVIS, R. H. 1990 On the buoyancy-driven motion of a drop towards a rigid surface or a deformable interface. *J. Fluid Mech.* **217**, 547–573.

YIANTSIOS, S. G. & DAVIS, R. H. 1991 Close approach and deformation of two viscous drops due to gravity and van der Waals forces. *J. Colloid Interface Sci.* **144**, 412–432.

YOUNG, N. O., GOLDSTEIN, J. S. & BLOCK, M. J. 1959 The motion of bubbles in a vertical temperature gradient. *J. Fluid Mech.* **6**, 350–356.

ZHANG, X. & DAVIS, R. H. 1991 The rate of collisions due to Brownian or gravitational motion of small drops. *J. Fluid Mech.* **230**, 479–504.

ZHANG, X. & DAVIS, R. H. 1992 The collision rate of small drops undergoing thermocapillary migration. *J. Colloid Interface Sci.* **152**, 548–561.

ZINCHENKO, A. Z. 1978 Calculation of hydrodynamic interactions between drops at low Reynolds number. *Prikl. Mat. Mech.* **42**, 955–959.

ZINCHENKO, A. A. 1980 The slow asymmetrical motion of two drops in a viscous medium. *Prikl. Mat. Mech.* **44**, 30–37.

ZINCHENKO, A. A. 1983 Calculations of the effectiveness of gravitational coagulation of drops with allowance for internal circulation. *Prikl. Mat. Mech.* **46**, 58–65.